LUND UNIVERSITY
Faculty of Science

Can blue mussel shells be used for retrospective ^{14}C-analysis in the marine environment of nuclear power plants?

Sofia Bjarheim

Thesis submitted for the degree of Bachelor of Science

Project duration: One semester, 15 credits

Supervisor: Kristina Eriksson Stenström

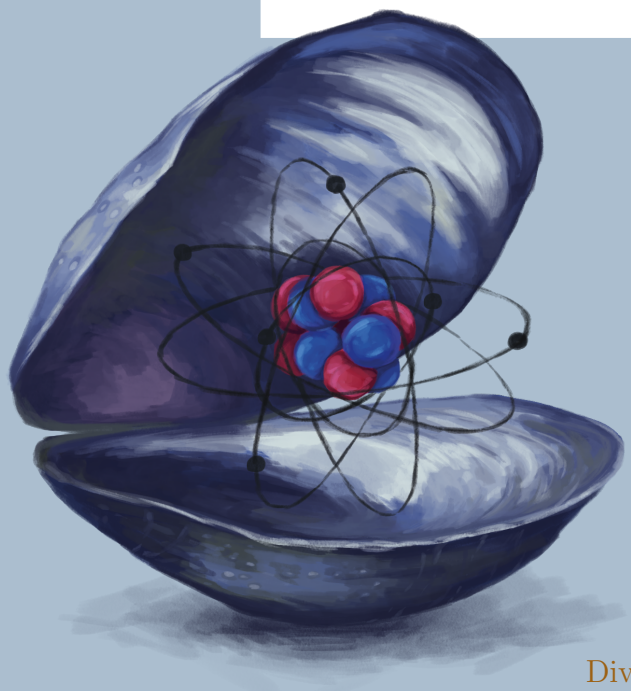

Department of Physics
Division of Particle and Nuclear Physics
January, 2024

Abstract

Carbon-14 (^{14}C) is one of the most important contributors to the collective effective dose of the public due to radioactive releases from nuclear power plants. However, the discharge of ^{14}C from nuclear power plants (NPPs) into water has not been measured previously. The aim of this project was to the develop a method for retrospectively analysing the annual discharge of dissolved inorganic ^{14}C. As the shells of blue mussels (*Mytilus Edulis*) form annual structures they can be used to acquire information about approximately the past ten years. The method developed within this project identified the annual rings and extracted samples from the shells, which are known to be built up of inorganic carbon from the habitat of the mussel. The ^{14}C content in the samples were analysed, and though the method still needs to be improved, the results were promising, and agree with previous studies on ^{14}C along the Swedish west coast.

Acknowledgements

First and foremost I would like to thank my supervisor Kristina Eriksson Stenström, who has been an amazing mentor and support throughout out this project. Krisitna has both guided me and allowed me enough freedom to find my own way of solving problems. I also want to give a huge thanks to Mattias Olsson and Anders Lindskog who have been crucial parts of the method development, I would not have been able to do it without your help. Another important person within this project is Per Carlsson, who helped us identify annual bands in the blue mussel, and helped me with finding good sources about blue mussels. I also want to thank Antonio Checa for taking the time to answer all my very specific question on shell structures, for which I could not find the answers to on google. Thank you to Git Klintvik Ahlberg and Ingemar Hansson who showed me around the Radiocarbon Dating Laboratory and explained what their work consist of. And lastly, thank you to my best friend, and graphic designer, Anina Rasmussen for making the amazing cover page illustration, more of her work is found at aninarasmussen.com.

This thesis is a part of the project *Radioecology of* ^{14}C *in the marine environment of Ringhals nuclear power plant* (project number SSM2022-4035) which is financed by the Swedish Radiation Safety Authority.

Abbreviations

AMS	Accelerator mass spectrometry
BWR	Boiling water reactor
DIC	Dissolved inorganic carbon
LWR	Light water reactor
NPP	Nuclear power plant
PWR	Pressurised water reactor
SSM	Swedish Radiation Safety Authority
SSAMA	Single-stage accelerator mass spectrometry

Contents

Chapter 1

Introduction

While most people might have heard that bananas are radioactive (Ji, 2022), ionising radiation as a concept is hard to visualise and hard to explain to someone with little prior knowledge regarding atoms. Since accidents at nuclear power plants can have devastating consequences, and because ionising radiation may be difficult to understand, it is often feared. Nonetheless, the nuclear industry is strongly regulated both on a national and international level, with regulations being updated continuously (SSM, 2023). Such an update is what initiated the need for this project. Starting from 1st of March 2022 Swedish nuclear power plants are required to measure their discharge of carbon-14 (^{14}C) into water during normal operation (SSMFS 2021:6), something that had not been done before. The aim of this Bachelor's project is to develop a way to retrospectively require some of this data.

This thesis will first give an introduction to the Bachelor's project as a whole, followed by a theoretical background. Thereafter, the method development, which was the main part of the project, will be explained. Then the results will be presented, and discussed. Lastly, the text will end with a conclusion and a future outlook.

In the currently enforced regulations regarding nuclear power plants, nuclide specific measurements of the discharge of ^{90}Sr, ^{14}C and ^{3}H into water is required (SSMFS 2021:6). However, the preceding regulations only stated that the discharge of ^{90}Sr and ^{3}H into water should be measured (SSMFS 2008:23). As mentioned there has been no measurements of marine nuclear emissions of ^{14}C done previously, and methods of measuring the marine discharge of ^{14}C have yet to be implemented (Stenström K. E., personal communication November 29th, 2023).

Retrospectively obtaining data on ^{14}C discharge have been done using blue mussel shells, which contain dissolved inorganic carbon (DIC) (Tierney, 2017). Since blue mussels develop annual patterns in their shells as they grow (Kautsky, 1982)yearly samples for up to 20 past years (Havforskningsinstituttet, 2021) can be acquired. During this project a method for identifying the annual patterns and extracting samples accordingly has been developed. With the future goals being: to estimate the past years' marine nuclear emissions of ^{14}C; make approximations of the radiation doses marine organisms have been subjected too due to ^{14}C; and, in the future, to use this method more extensively, with more individual samples from a greater amount of sample sites, to get a detailed picture of how the amount of ^{14}C along the coast of Sweden has changed in the past.

Other previous studies have used sea shells as proxy data, often *Arctica islandica* (which is a protected species in Sweden), the aim of many of said studies was to study the ^{14}C bomb pulse (Dunca et al., 2009; Schöne et al., 2005; Scourse et al., 2012). *Mytilus edulis* have also been used to study marine emissions of ^{14}C in the past, but the annual rings were not separated (Tierney, 2017). There are also several studies where the soft tissue of *Mytilus edulis* have been used to analyse marine emissions (Meli et al., 2008; Källberg, E., 2023; National Academy of Science, 1980). No previous studies of marine emissions of ^{14}C where the annual rings of mussels were separated were found.

Chapter 2

Theoretical background

In this chapter theory needed to properly follow the process of this project will be explained. Firstly focusing on the physics, before then explaining the shell structure of blue mussels, as this project is interdisciplinary involving both subjects.

2.1 ^{14}C in the environment

In the element carbon on our planet, three isotopes: ^{12}C, ^{13}C, and ^{14}C, are found. The most abundant, at 98.9% of all carbon, is ^{12}C, followed by ^{13}C at 1.1%, and then ^{14}C at about 10^{-10}% (see e.g. (Georgiadou, 2014)). Out of these three isotopes ^{14}C is the only radioactive one, and has a half-life of 5730 years. The isotope is also one of the biggest contributions to collective effective dose to the public (Stenström and Mattsson, 2022). This radioactive isotope is made naturally in the atmosphere when neutrons, produced by cosmic radiation, is captured by ^{14}N. There are also anthropogenic sources of ^{14}C, such as nuclear power plants (NPPs) and atmospheric testing of nuclear weapons. Reprocessing plants for spent nuclear fuel used in NPPs also emits ^{14}C, produced in the NPPs, into nature (see e.g. Magnusson, Å. (2007) and references therein). Testing of atmospheric nuclear weapons in the 1950s and 60s doubled the atmospheric ^{14}C and is known as the bomb-pulse or the bomb effect (Druffel and Suess, 1983). After atmospheric testing of nuclear weapons was banned, atmospheric levels of ^{14}C have decreased significantly. This is both due to CO_2 in the atmosphere being absorbed by the ocean, and due to emissions from fossil fuels, where all ^{14}C have decayed (Druffel and Suess, 1983).

The level of ^{14}C in the ocean varies both depending on the water depth and on the latitude (Druffel and Suess, 1983). Deeper in the ocean the proportion of ^{14}C will be smaller as much of it has decayed. On the other hand, the ocean currents in polar regions mix the water from different depths more quickly than in warmer latitudes, such that surface waters in the far north and south have less ^{14}C than surface waters in temperate and tropical latitudes (Druffel and Suess, 1983). Another reason for the increase of ^{14}C in the ocean is uptake of CO_2 in plankton, due to photosynthesis, this is released as the plankton dies and decays (Mæhlum, 2023). Furthermore, as the CO_2 levels in the atmosphere increases, the ocean will not be able to release as much CO_2, including ^{14}C, into the atmosphere (Mæhlum, 2023). Lastly it should be mentioned that, in coastal areas, rivers flowing into the ocean can also have a significant impact on the ^{14}C level in the ocean(Lougheed et al., 2013). Some rivers will increase the ^{14}C levels due to the CO_2 they have absorbed from the atmosphere, while other rivers may contain soluble bedrock, like limestone, leading to lower level of ^{14}C in the immediate area of the river outlet (Lougheed et al., 2013).

2.1.1 ^{14}C in nuclear power plants

There are several different types of reactors found in NPPs. However, all reactors in Sweden are Light-water-reactors (LWRs) (SSM, 2021a), and therefore only those will be discussed. There are two subcategories of LWRs, pressurised water reactors (PWRs) and boiling water reactors (BWRs). Ringhals, a Swedish NPP, currently has two operating PWRs, named *Ringhals 3*, which started operating in 1981 and *Ringhals 4*, which started operating in 1983 (Forsgren, 2012). The NPP also has two reactors which are no longer in operation, *Ringhals 1*, a BWR which was shut down in 2020, and *Ringhals 2*, a PWR shut down in 2019 (SSM, 2021b). The most common nuclear interactions for producing ^{14}C in both of the reactor types are found in Table 2.1. The ^{14}C created from ^{17}O and ^{14}N in the reactor water are the biggest contributors to emissions (Magnusson, Å., 2007).

Table 2.1: Production of ^{14}C within nuclear reactors (Magnusson, Å., 2007).

Reaction	**Natural isotope abundance of target element**	**Thermal cross section [barn]**
$^{17}O + n \rightarrow ^{14} C + \alpha$	0.038%	0.235
$^{14}N + n \rightarrow ^{14} C + p$	99.6%	1.82
$^{13}C + n \rightarrow ^{14} C + \gamma$	1.1%	$1.37 \cdot 10^{-3}$

.

PWRs are equipped with two different circulating water systems systems. The primary system, which is kept under high pressure and acts both as a cooler and a moderator, and a secondary system, which is heated by the first system and then used to power steam generators. This should in theory keep the secondary system free of radionuclides reducing radioactive emissions. Ocean water then cools the secondary system. It is important to note that the ocean water is not used within the secondary water system that produces the electricity (where steam passes through the turbine connected to the electrical generator), it is just a cooling liquid that does not mix with the reactor water (Forsgren, 2012). In PWRs the main reason for emissions of radionuclides would be a leakage between the two water systems in the reactor, as the secondary system is not filtered as thoroughly before being emitted into the surroundings (Reaktorkemi, 1974).

In BWRs there is only one water system, meaning that the same water used to cool the reactor is also used when powering the turbines. This water then goes through a filtering system with ion-exchange resins before cycled back into the reactor. However, this reactor water is also cooled using water pumped in from the ocean (Forsgren, 2012). While there are filters to catch any radionuclides present in possible fluid leakages from the reactor, this is still the main source of liquid discharges. Cooling water that leaks onto the power plant floor will also eventually be drained into the ocean (Reaktorkemi, 1974).

2.1.2 Units used in regards to ^{14}C

When plants and animals absorb carbon there is often a preference for certain isotopes, which means that the amount of ^{14}C observed in different organisms cannot be directly compared to one another. This is referred to as isotope fractionation (Georgiadou, 2014). Furthermore, it also means that the activity concentration [Bq kg^{-1} C^{-1}] of ^{14}C will be slightly higher in the air or water surrounding an organism, than it will be in the organism itself (Stenström et al., 2011). To balance this out, a normalisation factor is calculated based on the ratio between ^{12}C and ^{13}C in samples. When discussing this ratio, the term δ^{13}C is often used. By using these normalisation factors found for each sample, levels of ^{14}C can then be effectively compared (Stenström et al., 2011).

There exists an abundance of units used when measuring ^{14}C levels (Stenström et al., 2011).

For this project all values will be given as fraction modern, $F^{14}C$, calculated as

$$F^{14}C = \frac{A_{SN}}{A_{ON}}, \tag{2.1}$$

where A_{SN} is the normalised ^{14}C specific activity in the sample and A_{ON} is the specific activity of ^{14}C in a standard (normalised to $\delta^{13}C$ = -25 per mille). The specific activity of a sample, A [Bqkg^{-1}C^{-1}], is calculated as follows:

$$A = F^{14}C \left(\frac{\left(1 + \frac{\delta^{13}C}{1000}\right)}{0.975} \right)^2 e^{(1950-y)/8267} 226, \tag{2.2}$$

where y is the year of measurement.

2.2 Accelerator mass spectrometry

The samples in this project were analysed using accelerator mass spectrometry (AMS). Since ^{14}C has such a long lifetime, it is impractical and time-consuming to measure it by counting the number of decays. Traditional mass spectrometers are also of little use, since the ^{14}C atoms are indistinguishable from other atoms and molecules with approximately the same weight as ^{14}C, so called isobars, such as ^{14}N and $^{12}CH_2$ (Fifield, 2005). The accelerator used at the radiocarbon dating laboratory in Lund is a single-stage accelerator mass spectrometer (SSAMS)[1] (Skog, 2007), and is depicted in Figure 2.1.

Before samples can be analysed in the accelerator they go through a pre-treatment, which involves cleaning the samples and extracting the samples as graphite (Hansson, I., personal communication November 22nd, 2023; Ahlberg, G.K., personal communication November 29th, 2023). This process may differ depending on the sample material (Hansson, I., personal communication November 22nd, 2023). The exact method that was used when treating the samples from this project is described in sections 4.1 and 4.2.

2.2.1 Single-stage mass accelerator spectrometry

After the graphite samples are put into the SSAMS, step one of the acceleration process is to turn the graphite into C^--ions, which is done in the ion source, containing Cs^+-ions (location 1 in Figure 2.1). Additionally, turning the sample into negative ions guarantees that the isobar ^{14}N will not interfere with the measurement of ^{14}C, since ^{14}N can not form negative ions (Weisser, 2013). The negative carbon ions are then accelerated by an electric field, gaining an initial energy of about 40 keV (Fifield, 2005; Weisser, 2013). Next the ions are directed through an electrostatic analyser (location 2), which selects the ion source (there are two ion sources in the SSAMS system) and improves the energy resolution of the ion beam (Stenström (2015) and sources therein). After this the ion beam will be bent 90° by a dipole magnet kept at a constant magnetic field (location 3 in Figure 2.1). A charged particle travelling through a magnetic field will change its trajectory, the radii, R, of the path at which a particle is bent is described by the following equation

$$R = \frac{mv}{qB} = \frac{\sqrt{2mE}}{qB}, \tag{2.3}$$

where m is the mass of the particle, v is its velocity, q is its charge, B is the strength of the magnetic field, and E is the energy of the ions. At this stage all the ions have charge -1 e, and their energies are the same.

[1] Fun fact: It was built in 2004 and is the first SSAMS accelerator in the world (Skog, 2007).

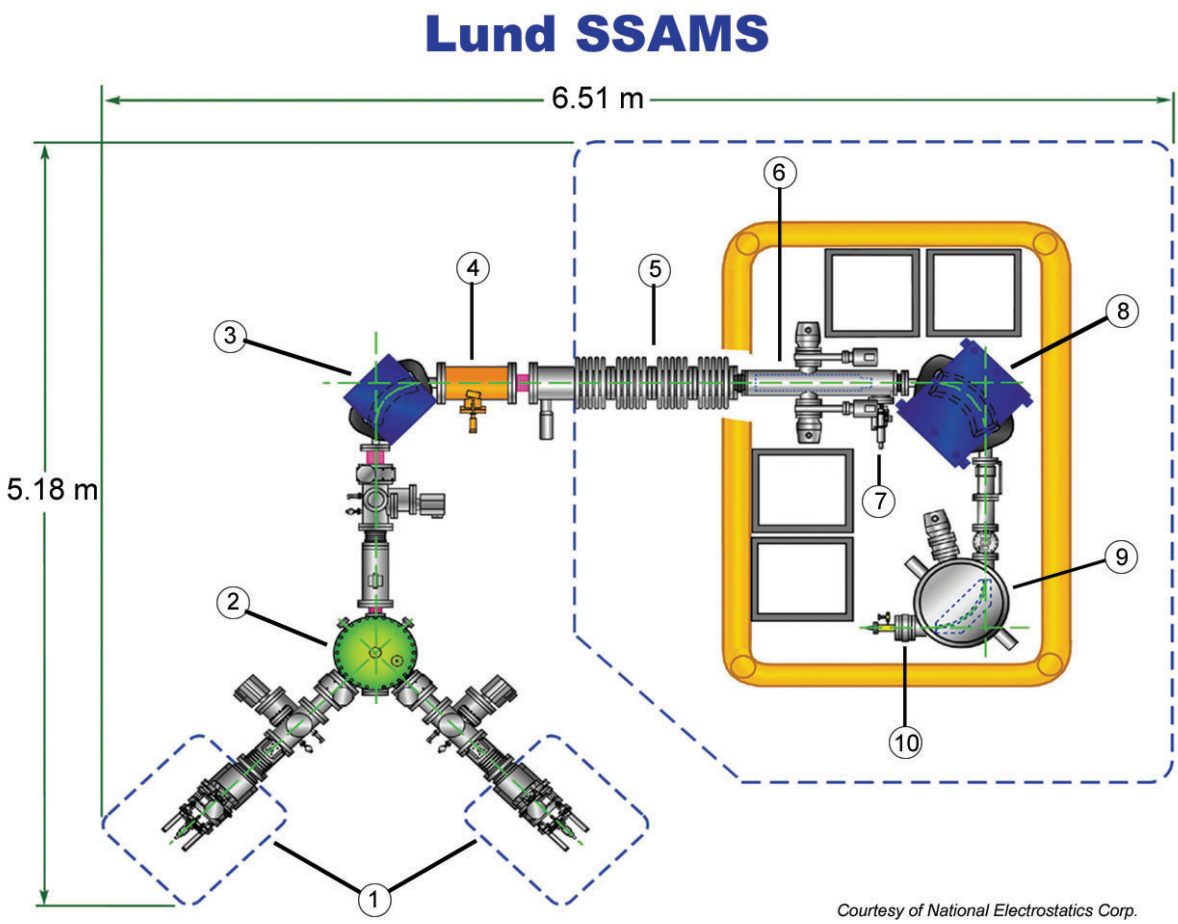

Figure 2.1: A schematic illustration of the SSAMS in Lund. Used with permission from the *National Electrostatics corp.*

Since ^{12}C, ^{13}C, and ^{14}C have different masses, the electric field in-between the electrostatic analyser at 2 and the dipole magnet at 3 will change voltage several times a second, giving the isotopes different energies. Thus alternating which of the isotopes makes it through the bend (Fifield, 2005). More time will be spent letting the ^{14}C ion beam pass, compared to the other ions (Klody et al., 2005), since ^{14}C is the least abundant. At location 4 in Figure 2.1 there is an Einzel lens, which uses equipotentials to focus the ion-beam (Stenström (2015) and sources therein). Then at location 5 there is a second accelerator providing the ions with an additional energy of of 250 keV. Next (at location 6) the ions will go through a stripper filled with He, breaking apart any molecules left in the beam and giving the ions a positive charge, for this process the potential of 250 keV is needed (Hansson, I., personal communication November 22nd, 2023), location 7 in Figure 2.1 marks the stripper gas valve. After the stripper (location 6) follows one more 90° dipole magnet, kept at constant magnetic field (location 8). Here the ^{12}C, ^{13}C, and ^{14}C ions are separated and the ^{12}C and ^{13}C ions are detected using Faraday cups located off axis after the dipole magnet at location 8. At 9 in 2.1 the ^{14}C ions goes through another electrostatic analyser. At location 10 there is a sequential post-accelerator deflector, an electrical field that filters the ions making sure that essentially no other ions than ^{14}C hit the detector, as it will break if it is hit with too strong of a current (Stenström, K. E., personal communication December 11th, 2023). Lastly there is the ^{14}C detector, a silicon semiconductor with a pn-junction (Hansson, I., personal communication November 22nd, 2023).

2.3 Blue mussels

Blue mussels, or *Mytilus edulis*, are seashells common in the northern parts of the Atlantic Ocean. Terms used when indicating different regions of their shells, which will be used in this text, are shown in Figure 2.2. Blue mussels survive in harsh conditions, filter through up to five litres of sea water per hour, and can live up to 20 years (Havforskningsinstituttet, 2021). However, a British study, which looked at the ages of blue mussels within several mussel beds, found that a big proportion of blue mussels do not survive past the first two years. Additionally this study found that between the age of four and seven years the relative density of mussels within the age group started to decline (McGrorty and Goss-Custard, 1993). It would therefore be unreasonable to expect finding many mussels which are twenty years old. Along the Swedish west coast it is uncommon to find blue mussels older than ten years (Carlsson, P., personal communication November 30th, 2023).

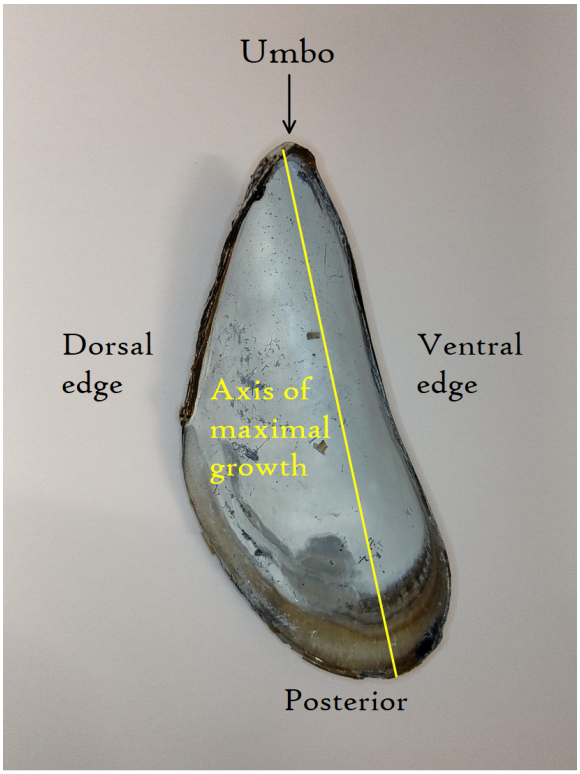

Figure 2.2: Terms used when indicating different parts of mussels according to Dalbeck (2007).

The shells of blue mussels are in large part grown from dissolved inorganic carbon (DIC). The main food source for blue mussels, which partly contributes to the material used during shell formation, is phytoplankton which get all their carbon from DIC (Tierney, 2017).

2.3.1 Structure and growth of shell layers

The shells of mussels consist of three layers, the periostracum, the fibrous- or prismatic layer and the nacre (Checa and Salas, 2017). These three shell layers are illustrated in Figure 2.3. Note that, the term prismatic layer normally refers to a thicker layer of individual crystal structures with organic membranes in between, where crystals are perpendicular to the growth surface. This can be seen in other bivalves, such as oysters. The fibrous layer is instead made of thinner calcite fibres, with an inclination of about 45° in relation to the growth surface, this is seen in blue mussels. It was therefore advised by Antonio Checa, professor in palaeontology at the University of Granada, to rather refer to this layer as the fibrous layer (personal communication, October 11th, 2023).

The periostracum is an organic layer which is created by the mantle in the periostracal groove. Where the periostracum forms it seals the seawater off, making biomineralisation possible. The region where biomineralisation happens is called the extrapallial space (Checa and Salas, 2017). Both the fibrous layer and the nacre are made of calcium carbonate ($CaCO_3$), but the two layers have different crystal structures. The fibrous layer has the structure of calcite and the nacre has the structure of aragonite (Dalbeck, 2007). The annual structures within these two shell layers does not align with each other, something which was seen in the acetate peels (explained in section 3.1) made during the method development. In these it was seen that the annual structures in the two layers were not parallel in the cross sections of the shells. Pictures showing this is presented in Figures 3.3 and 3.4.

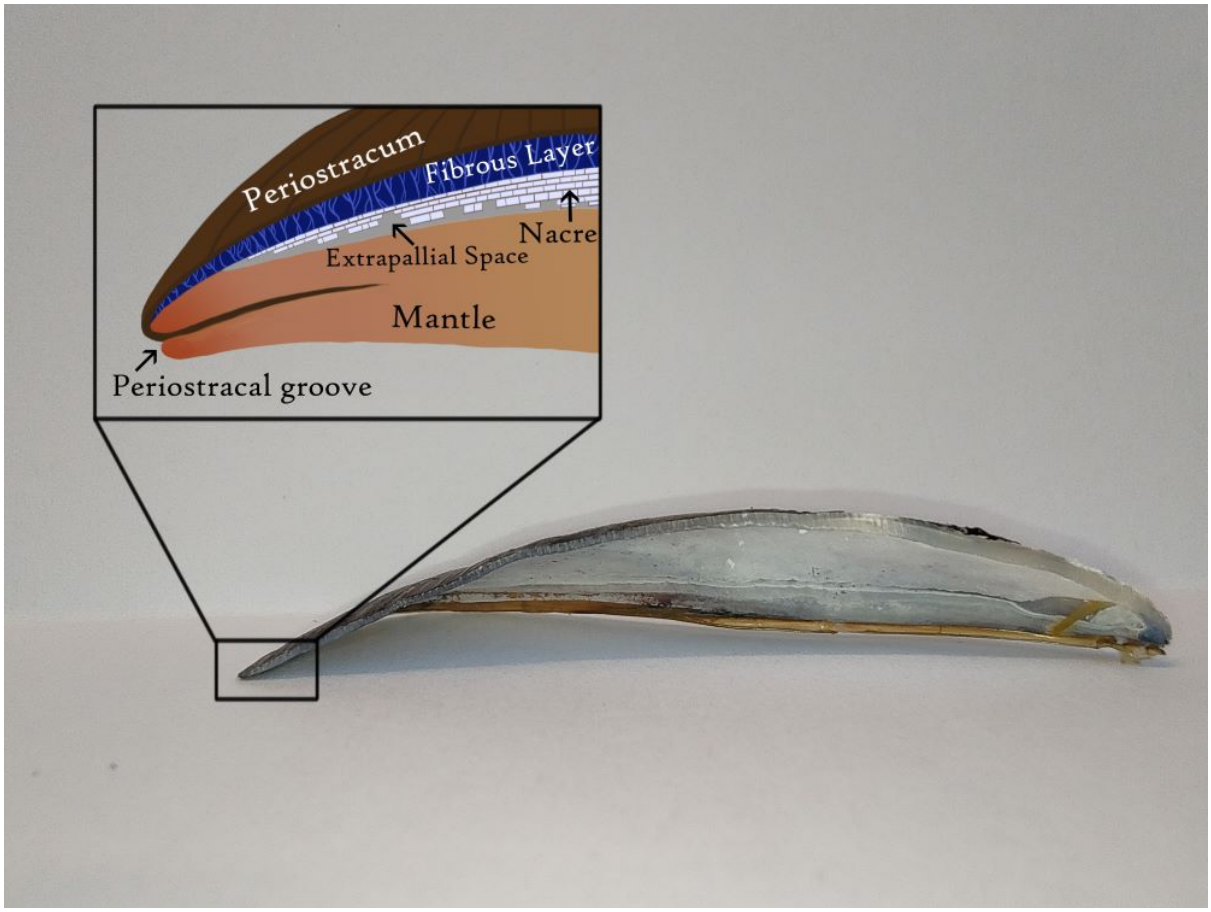

Figure 2.3: Blue mussel shell with an illustration of the different shell layers. Note that the drawn structure of the fibrous layer should have been more diagonal in comparison to the other layers. The mantle, depicted in peach in the illustrated insert, is part of the soft tissue and not seen in the picture. Based on Figure 2 from (Checa, 2018) recreated with permission from the author.

As mentioned, blue mussels form annual growth rings, it is however uncertain at what time of the year these are formed. Some theories connect the the formation of growth rings to the winter, when the temperatures are colder and less food is available. Other theories connect the formation to the spawning periods of the mussels (Kautsky, 1982). However, it is agreed upon the fact that annual structures forms as a result of a period with slow growth of the shell. For blue mussels in the northern Baltic Ocean, along the east coast of Sweden, there is a consensus that growth rings are formed during winter (Kautsky, 1982), it would not be unreasonable to assume that the same is true for blue mussels along the west coast of Sweden.

Chapter 3

Method development in regards to blue mussel shells

The method development was essentially the main part of this thesis project. It was also the most time consuming part. Firstly, methods used in similar projects were studied and the possibility of using those for this project was considered. It was found that methods where the shell age was determined often involved embedding the shells in epoxy (Clark, 1980; Dunca et al., 2009; Schöne et al., 2005; Neves and Moyer, 1988; Haag and Commens-Carson, 2008; Henley and Jones, 2020). It was also concluded that studies concerning the effect that environmental factors and pollutants have on blue mussels were generally focusing on the soft tissue (Connan and Tack, 2010; Meli et al., 2008; Källberg, E., 2023; National Academy of Science, 1980). Since the aim of this Bachelor's project was to study the amount of ^{14}C occurring in blue mussel shells, epoxy could not be used without risking contamination of the samples with carbon from the epoxy. The studies regarding the soft tissues did not have any methods that were directly applicable to studies of the shells.

Due to this, a method had to be developed specifically for this project. The first step of the development was to identify the main segments of the process. One part was to find the age of the blue mussels and identify the location of each annual ring. Another part was to be able to divide the shells according to these rings, with the last part being to separate the nacre from the fibrous layer.

3.1 Blue mussel age and annual rings

As a first step, known ways to identify annual patterns in mussel shells were researched and three common approaches were identified. The methods found included thin sectioning (Clark, 1980; Rypel et al., 2008), identification of visible external patterns on the shell valves (Kautsky, 1982; Neves and Moyer, 1988), and making acetate peels (Kennish et al., 1980; Lutz, 1976).

Thin sectioning entails cutting out a slice of shell along the axis of maximal growth, and sanding it down until it is thin enough to allow light to shine through, about 50-100 μm. The section is then studied using a microscope (Clark, 1980). While this is regarded as the most reliable method for identifying the annual rings (Neves and Moyer, 1988), it takes a lot of practice to be able to do it well and the method is time consuming (Clark, 1980). A further issue is that if a mistake is made when producing the thin sections, it is likely that the process has to be started over, using a new shell piece. Considering that parts of the shells, taken along the axis of maximal growth, were needed for taking samples (see the middle section in figure A.1 in the appendix) it would also be hard to make a thin section which included all the annual structures, without using to much of the sample material.

Identifying the annual patterns of the shell valves externally became the main approach for deciding the age of the blue mussels, as it did not require as much prerequisite knowledge

of sample preparation techniques as the other methods. With the aid of a strong lamp, the identification of the annual bands becomes significantly easier (Kautsky, 1982), since the border between two growth seasons appears darker than the neighbouring shell. During preliminary testing, it was concluded that for young, thin, blue mussel shells the annual growth rings can be clearly seen. However, older shells, which are thicker, will be harder to determine the age of using this method. To make the age determination easier the periostracum was sanded off the shells, which lead to more light shining through the blue mussels. An illuminated shell with the periostracum sanded away can be seen in Figure 3.1. It should be noted that after heating (another step of the method, see below) the shells would let less light through when illuminated. Therefore, the location of the annual rings were marked before heating.

Figure 3.1: Picture of an illuminated blue mussel (lenght 56 mm) with its periostracum removed, taken during initial testing. Towards the ventral edge of the shell valve, part of the fibrous layer is eroded.

Acetate peels of the samples were also made, one of which can be seen in Figure 3.2. An acetate peel is a replica of the cut edge of a shell, cast onto a cellulose film (Kennish et al., 1980). A step by step description of the method used to make the peels is found under point 4 in Appendix A. While it is common practice to cast bivalves in epoxy before making the acetate peels (Kennish et al., 1980; Lutz, 1976) this was not done here as to avoid contamination,

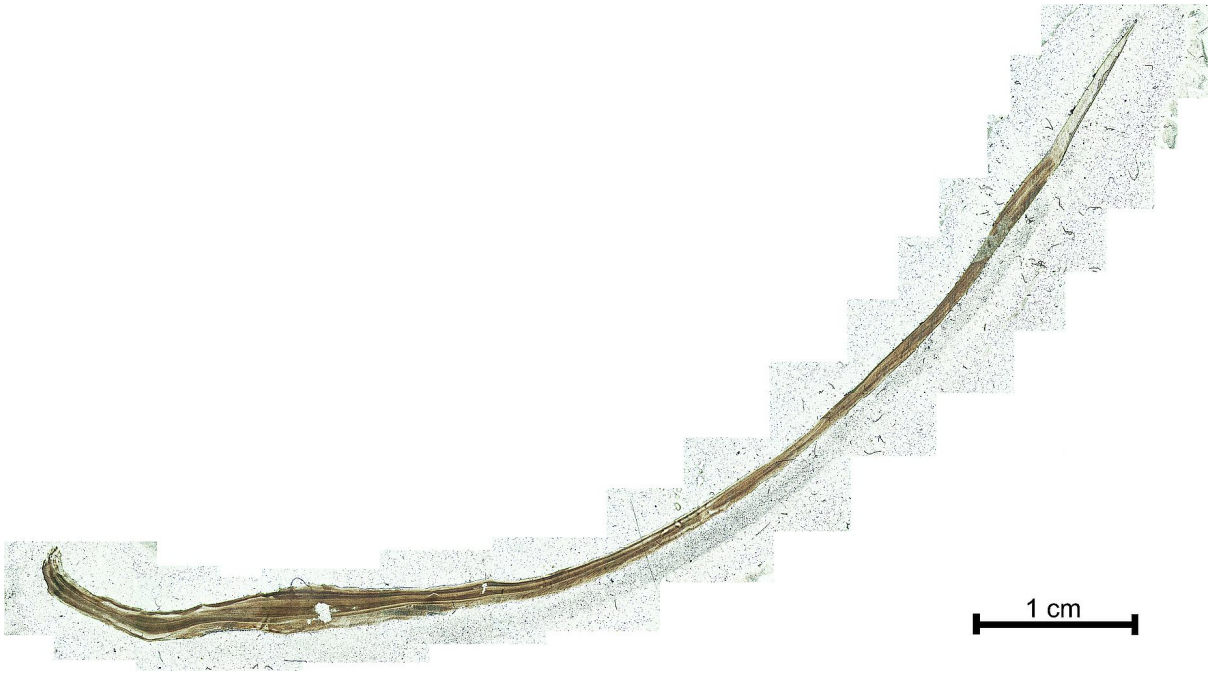

Figure 3.2: Panoramic picture of an acetate peel seen under a microscope, with the umbo-region in the lower left corner and the posterior edge in the upper right corner. The colour and saturation of the picture are edited to make the shell structure appear more clearly. Picture by Anders Lindskog.

and the resulting peels were still of very good quality. Furthermore, they had a similar amount of detail compared to the thin sections depicted in literature (e.g. in (Lutz, 1976)). Another advantage with the acetate peels is that several peels can be created from the same shell without loosing a significant amount of material.

In the acetate peels annual layers parallel to the surfaces of each shell valve were clearly visible in the umbo region of the nacre, as seen in Figure 3.3. Towards the posterior edge of the shell, where only the fibrous layer had been formed, annual structures more diagonal to the shells were observed, shown in Figure 3.4. It is also apparent, that the fibrous layer extends further than the nacre, something that can be clearly seen in Figure 2.2. All three observations agrees with the two shell layers not growing in parallel.

The number of layers seen in the nacre was compared to the number of layers seen when illuminating the shells. Then the locations of annual rings in the fibrous layer found in the acetate peels were then compared to the location of the markings drawn on the outside of the shell.

There is also a fourth way to determine blue mussel age, comparing the shell size to growth curves (Seed, 1980). Such curves are

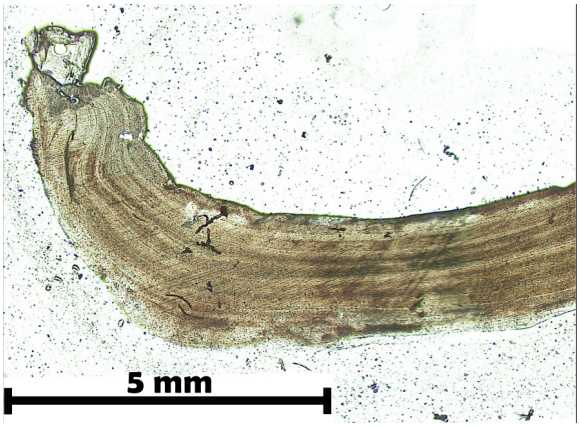

Figure 3.3: Acetate peel depicting the umbo region of a blue mussel from Särdal. Picture by Anders Lindskog.

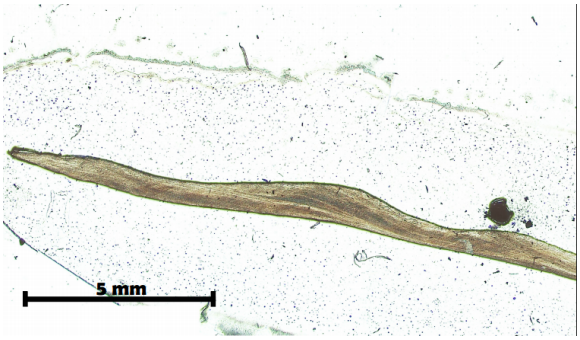

Figure 3.4: Acetate peel depicting the posterior edge of a blue mussel from Särdal. Picture by Anders Lindskog.

based on the assumption that a given species have a maximal attainable size that they cannot surpass. Since *Mytilus edulis* varies significantly in size based on growth conditions, such as temperature and ocean salinity, a growth curve for similar conditions have to be found before size comparisons can be made. This method of determining the mussel age is not able to locate annual bands and will only give an estimate of the total age of each mussel. Comparing the sizes of the blue mussels from this project to growth curves was only done after the sample preparation using pictures of the shells to determine the sizes of each annual band. In future studies this will be done as a part of the sample preparation. The reliability of the methods used to determine the ages of the blue mussels will be discussed below in section 6.1.

3.2 Cutting up the shells and dividing the annual rings

Cutting the blue mussel shells was somewhat challenging due to their brittleness, and several approaches were tested. To better be able to separate the calcium carbonate layers of the shell, something that will be explained later, the dorsal and ventral edges of the shells were cut off, using a lapidary saw. Thus creating a triangular middle piece (shown in the appendix in Figure A.1) which would later be divided into samples according the annual bands. In agreement with Sterrett and Saville (1974), it was found, when heating an uncut shell, that the shell layers were harder to separate along the dorsal and ventral edges.

After extracting the middle piece, acetate peels were made from it and analysed. Specifically

they were created using the cut facing the ventral edge, as it was the closest to the axis of maximal growth. Subsequently, the triangular middle parts of the shells were cut into pieces according to their annual rings, using a Dremel with a diamond blade rotating on slow speed. A shell cut according to its annual rings is seen in Figure 3.5.

Figure 3.5: Shell from Båteviken cut according to its annual rings.

3.3 Separating the shell layers

As described in section 2.3.1, the annual structures in the fibrous layer and the nacre do not align. Due to this it was decided that only one of the layers would be used in the ^{14}C-analysis, something that was also recommended by Antonio Checa (personal communication, October 11th, 2023). Since the annual structure of the nacre forms in thin sheets, which would be hard to individually separate from each other, the fibrous layer was used for the final samples.

A possible way to separate the shell layers would be to grind away the unwanted shell. This method has been used with success on bivalves of the species *Arctica islandica* (Scourse et al., 2012; Weidman and Jones, 1993). However, due to the brittleness of the blue mussels and the fact that the fibrous layer is relatively thin in comparison to the nacre, tests of grinding away the nacre failed.

The solution was instead to separate the layers by heating the shells in an oven with air at 500 °C for 10 minutes. On shells of other bivalves, heating is documented to achieve separation of annual layers (Tevesz and Carter, 1980; Sterrett and Saville, 1974). No sources were found where such a approach had been tested on blue mussels. Furthermore, Neves and Moyer (1988) found that this technique was unable to properly separate all layers, it also ended up making the freshwater mussel shells they used extremely brittle.

The first tests of heating proved that it did indeed make the shells more brittle. However, it also separated the nacre from the fibrous layer and most of the periostracum was burned away. For this initial attempt the shell

Figure 3.6: A shell from the initial testing, showing the separation of layers. Heated from about 400 °C to 500 °C, taking approximately 12 minutes.

was not cut previously mentioned, and it was noted that the layers did not separate well along the posterior and anterior edges, which coincides with the observations by Sterrett and Saville (1974). When the shells were cut as according to Figure A.1 the nacre and fibrous layer separated easily, as seen in Figure 3.6.

Several different temperatures and burn times were tried out, described in Table 3.1. Using a hot air gun to heat the mussels was also tested, but it did not reach sufficient temperatures. It was found that the periostracum was scorched off at around 450 °C. Furthermore, heating the shells at 600 °C made them noticeably more brittle than at 500 °C. Moreover, it was concluded that heating the shell for a shorter period, about 2 min, made it harder to separate the nacre and fibrous layer. At the same time there was no clear advantage to heating the shells for too long either, no significant difference was seen between shells that had been heated for 10 minutes and those that had been heated for about 30 minutes. After several tests it was decided to heat the shells for 10 minutes at 500 °C.

It was hard to discern if all the nacre was separated from the fibrous layer after heating. The inside of the fibrous layer, which had been connected to the nacre, had a rather shiny surface, as seen in Figure 3.7. Attempts to sand this shiny layer away were made, but this was given up on for two reasons. Since the shells turned more brittle after heating, all attempts of sanding led to the shells cracking into small pieces. Secondly, it was hard to judge if the possible nacre was removed or if the surface had just become matte due to the sanding. Therefore it was decided to remove this using weak acid. However, when doing analysis of shells, the ^{14}C lab in Lund usually treats shell samples with acid, therefore this part was left to them.

Table 3.1: Notes from the shell heating tests.

Temperature	**Duration**	**Comment**
240 °C → 500 °C	25 min	Less brittle compared to 600 °C. Layers separated.
400 °C → 500 °C	12 min	Wide shell section (as in Fig. A.1). Periostracum seemed to burn away at ca. 450 °C. Less smoke as compared to putting in the shells directly at 600 °C. Layers separated.
400 °C → 500 °C	12 min	Narrow shell section. Harder to handle without breaking than the wider section. Otherwise similar results.
420 °C	15 min	Less brittle than when heated at 500 °C. Still some periostracum left on the shell.
420 °C	27 min	Same results as when heated for 15 min at 420 °C.
500 °C → 600 °C	2 min 30 s at 600 °C	Harder to separate the shell layers. The colour of the fibrous layer turned more grey compared to lower temperatures.
500 °C → 600 °C	11 min 30 s at 600 °C	The layers separated like before. There seemed to be as much assumed nacre left compared to heating for the same amount of time at 500 °C.
600 °C	5 min	Possibly more of the nacre separated from the fibrous layer. The shell got so brittle it was hard to work with. It possibly broke along an annual ring in the fibrous layer, however this was hard to say for certain.

3.4 Summary of the method for extracting annual samples of blue mussel shells

Firstly the periostracum was sanded away, and then the location of each annual ring was found and marked, with the help of a bright light source. The dorsal and ventral edges of the shells were then cut off and acetate peels were made. The annual structures seen in the acetate peels were then compared to the markings made on the outside of the shells. Following this the shells were divided annually according to the markings made on the outside of the shells. Lastly the shells were heated at 500 °C for 10 minutes and the fibrous layer of each annual sample was sent to the ^{14}C lab to be treated with weak acid, 10 ml of 37% HCl diluted to 1000 ml with distilled water, and then converted to graphite and analysed by SSAMS. The sample treatment done at the ^{14}C lab is described in detail in Chapter 4. A full step by step description of the method is found in Appendix A and B.

3.5 Sampling sites

The samples used for the analysis were taken from three sample sites along the Swedish west coast shown in Figure 6.1. The samples from the site in Särdal (56.76 N, 12.63 E) were collected on the 24th of December 1978 (collected by professor Sören Mattsson, Medical Radiation Physics, Malmö, Lund University) and therefore significantly older than the other samples. The mussels from Båteviken (58.95 N, 11.13 E) were collected on the 12th of October 2022, the mussels from Bua (57.24 N, 12.10 E) were collected on the 12th of May 2023. All blue mussels were collected alive, by hand, in shallow waters. Several blue mussels were picked from each site, and samples from two of them were analysed by SSAMS. Details regarding the samples are presented in Table C.1.

The ^{14}C content of the blue mussels are be compared to seaweed (*Fucus vesiculosus*), which also accumulates DIC, and grass, which shows the level of ^{14}C in the air. Data from a few of the samples used for comparison are published by Stenström and Mattsson (2022), but the bigger portion is from so far unpublished. This unpublished data is from the SSM 2022-435 project, funded by the Swedish Radiation Safety Authority (SSM).

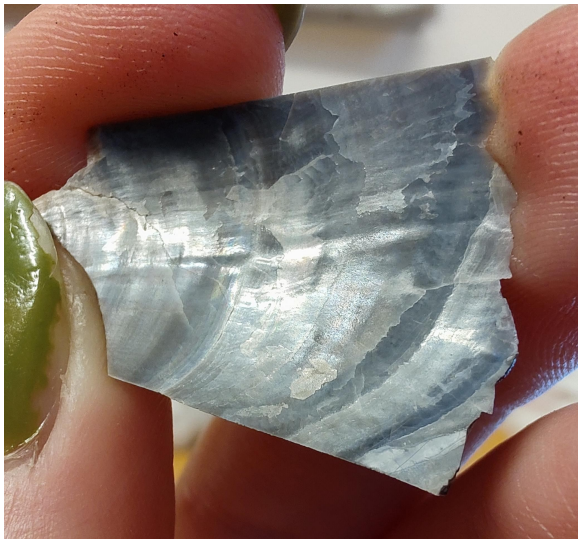

Figure 3.7: The inside of the fibrous layer after the shell had been heated.

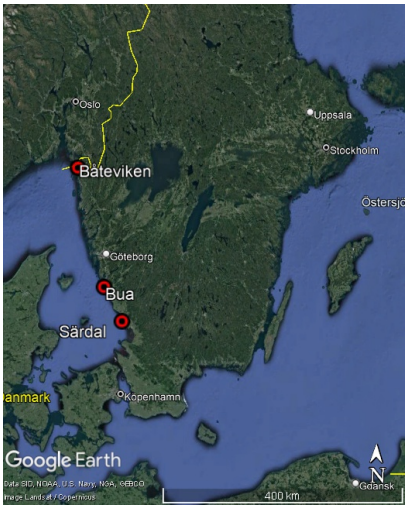

Figure 3.8: Map of the south of Sweden with the sample sites marked. Bua is close to Ringhals NPP.

Chapter 4

^{14}C analysis at the Radiocarbon dating laboratory in Lund

All information information in this chapter is based on standard procedures at the radiocarbon dating laboratory in Lund, and the work mentioned was done by personnel there[1]. When sending in samples for ^{14}C analysis all of the following parts of the sample treatment, as well as the SSAMS measurent is done by personnel at the lab. It is explained here for the sake of making all steps of this project transparent to the reader.

4.1 Acid treatment for shell and carbonate samples

After registering the samples in an internal filing system, samples are weighted, and then thoroughly cleaned. Samples are both brushed and ultrasonically washed (Ahlberg, G.K., personal communication November 29th, 2023). Following this the samples are put in a weak acid consisting of 10 ml of 37% HCl, which have been diluted to 1000 ml with distilled water (Ahlberg, G.K., personal communication November 29th, 2023). The amount of acid a shell is put into depends on it's weight and is listed in Appendix B. The acid solution with the shell, is then put in an oven with air at 80 °C for about 3 hours, this removes any organic material left on the shells (Ahlberg, G.K., personal communication November 29th, 2023). The shells are again ultrasonically washed, and then dried (Ahlberg, G.K., personal communication November 29th, 2023). A step by step description of the method is included in Appendix B.

4.2 Graphitisation

Before a sample can be analysed by AMS it has to be graphitised (Fifield, 2005). Firstly the sample is turned into CO_2, in the case of seashells this is done by letting the shells react with phosphoric acid, but in other cases it can be done by combustion (Hansson, I., personal communication November 22nd, 2023). The CO_2 is then mixed with hydrogen and heated to 600 °C in an oven together with an iron catalyst, forming graphite and H_2O. The graphite, and the iron which is left, will lay in the bottom of the heated tube where the reaction happened, the H_2O rises to the top where it is cooled and turned into ice. The ice is then separated from the rest (Wacker et al., 2010). Following this, the graphite is pressed into small capsules and put into the accelerator sample wheel, which can hold 40 samples (Hansson, I., personal communication November 22nd, 2023). At this point the samples usually weight between 700 to 800 μg, but samples as small as 100 μg can be analysed (Hansson, I., personal communication November 22nd, 2023).

[1] I was very kindly allowed to observe much of this as to better understand the process myself.

4.3 SSAMS measurement

The first step of the acceleration process, after the sample wheel has been put into place, is to pump a vacuum within the chamber containing the samples and ion source (the remaining interior of the accelerator is always kept at a vacuum) (Hansson, I., personal communication November 22nd, 2023). The samples are usually put into the accelerator during the afternoon, so that the vacuum pump can run all night before making the measurements. Afterwards, the ion beam is adjusted to optimise the measurements, this is done while observing the ^{13}C-ions due there being too few ^{14}C-ions and too many ^{12}C-ions for effective optimisation (Hansson, I., personal communication November 22nd, 2023). The theoretical maximum left of the beam after having passed through the stripper is 52% (Hansson, I., personal communication November 22nd, 2023). It is important to avoid having the ^{12}C- and ^{13}C-ions hitting the ^{14}C detector, as it can only handle very low currents and will break if it is hit by the ^{12}C or ^{13}C beams (Hansson, I., personal communication November 22nd, 2023). The individual carbon atoms hitting the detectors are plotted in a histogram. The samples are usually measured 18 times, with each measurement lasting for 160 s. Most of the time is spent measuring ^{14}C (Hansson, I., personal communication November 22nd, 2023). The sample wheel also contains a numbers of standards (presented in Table 4.1) to which the measurements are compared (Hansson, I., personal communication November 22nd, 2023; Ahlberg, G.K., personal communication November 29th, 2023). The uncertainty for the measurements can be approximated by the square root of the number of measured ^{14}C-ions, meaning that more active samples will have a lower uncertainty (Stenström, K. E., personal communication December 11th, 2023).

4.4 Data Analysis

After the accelerator run the results are analysed by personnel at the radiocarbon dating laboratory (Stenström K. E., personal communication November 9th, 2023). And compared to standards called OX I, OX II, C1, C7 and C8 (Ahlberg, G.K., personal communication November 29th, 2023). The results are then sent out to clients in files such as shown in Figure 4.1.

Table 4.1: $F^{14}C$ of the standards used. C1, C7 and C8 are from IAEA (2014) and the uncertainties are given within the parenthesis, OX-I and OX-II are from Stenström et al., (2011) (where no uncertainties where given).

Name	**Material**	**$F^{14}C$**
C1	Carbonate (marble)	0.0000(02)
C7	Oxalic acid	0.4953(12)
C8	Oxalic acid	0.1503(17)
OX-I	Oxalic acid	1.0398
OX-II	Oxalic acid	1.3408

Dateringsattest

Provets benämning	Lab no	^{14}C-ålder BP	Provmgd (mg C)	Förbehandling
Bua Bua_230512_mussla2_år1	LuS 19291	2.126 ± 0.008 fM	1,0	7% avlägsnat med HCl
Bua Bua_230512_mussla2_år2	LuS 19292	1.313 ± 0.006 fM	1,0	8% avlägsnat med HCl
Bua Bua_230512_mussla2_år3	LuS 19293	1.275 ± 0.006 fM	1,0	13% avlägsnat med HCl
Bua Bua_230512_mussla2_år4	LuS 19294	1.722 ± 0.007 fM	1,1	29% avlägsnat med HCl
Bua Bua_230512_mussla2_år5	LuS 19295	1.233 ± 0.005 fM	1,1	27% avlägsnat med HCl

Figure 4.1: An example showing part of the dating certificate from The Lund Radiocarbon Dating Laboratory for shell samples from this project.

Chapter 5

Results

The $F^{14}C$ results of the shell samples analysed by SSAMS are listed in Table C.1. The plots presented below were produced using Python, and only include the analytical uncertainties from the ^{14}C analysis and not the uncertainties of the estimation of the year a mussel sample is from. The reason for not including these uncertainties in the plots was due to them being hard to quantify with exact numbers, something that will be discussed further in Chapter 6.

5.1 Validation of age estimates

Figure 5.1 compares the length of annual bands from the samples of this project to results from Dunca and Boalt (2011). This was done as a further measure to estimate the ages of our mussel samples. Dunca and Boalt (2011) looked at the relationship between the lengths of blue mussels and their age at various sites along the Swedish coasts. One of these site, Kullen, has similar environmental conditions as the samples sites in our project. Dunca and Boalt (2011) present the data by total mussel length and mussel age, meaning that the plot for this data is based on several mussels from the same sample site, and was not acquired by measuring the distance between growth bands for single mussels, as was done in this Bachelor's project. In the data from Dunca and Boalt (2011) there were several ages for which more than one mussel were picked, in Figure 5.1 the average mussels length for these ages are plotted. The length of mussels found by Högby fyr on Öland, by the Swedish east coast are also shown to emphasise the effect growth conditions have on the mussel size. It should also be noted that in the original data from Dunca and Boalt (2011) the first year of the mussel lifespan is counted as year zero, this is called year one in Figure 5.1 to be in agreement with the data from this project.

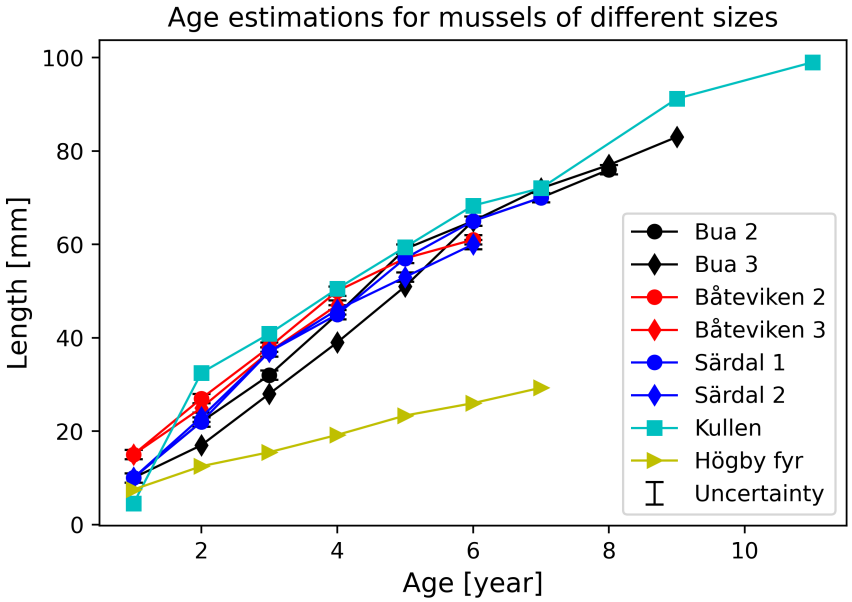

Figure 5.1: Length of each yearly segment from the mussel shell samples, compared to mussel from Kullen, a location with similar salinity and temperature as our sample sites and Högby fyr, a location with different conditions. Data for Kullen and Högby fyr is from Dunca and Boalt (2011). The error bars shows the uncertainty in she size measurement of each growth band in our samples.

5.2 Blue mussels from Båteviken and Bua

Figure 5.2 depicts the $F^{14}C$ in shells of blue mussels from Båteviken and Bua, the latter being the sample site by Ringhals NPP. The plot also includes $F^{14}C$ from seaweed *(Fucus vesiculosus)* growing at each of the sample sites, and grass growing on the coast nearby. Most of this is unpublished data, except the seaweed samples taken at both sites in 2020, which is from Stenström and Mattsson (2022). Values for the seaweed and grass samples are presented in Table 5.1, for values for the blue mussel shells see Table C.1.

Table 5.1: Data from seaweed and grass, data marked with an asterisk have been published by Stenström and Mattsson (2022).

Sample	**Date picked**	**$F^{14}C$**
Seaweed Båteviken	* 2020 Apr. 04	1.906(8)
	2022 Oct. 12	1.053(5)
	2023 May 4	1.056(5)
Grass Båteviken	2022 Oct. 12	1.013(5)
Seaweed Bua	* 2020 Mar. 31	1.322(7)
	2022 Oct. 13	1.310(6)
	2023 May 5	1.230(5)
Grass Bua	2022 Oct. 13	1.009(5)
	2023 May 5	1.004(5)

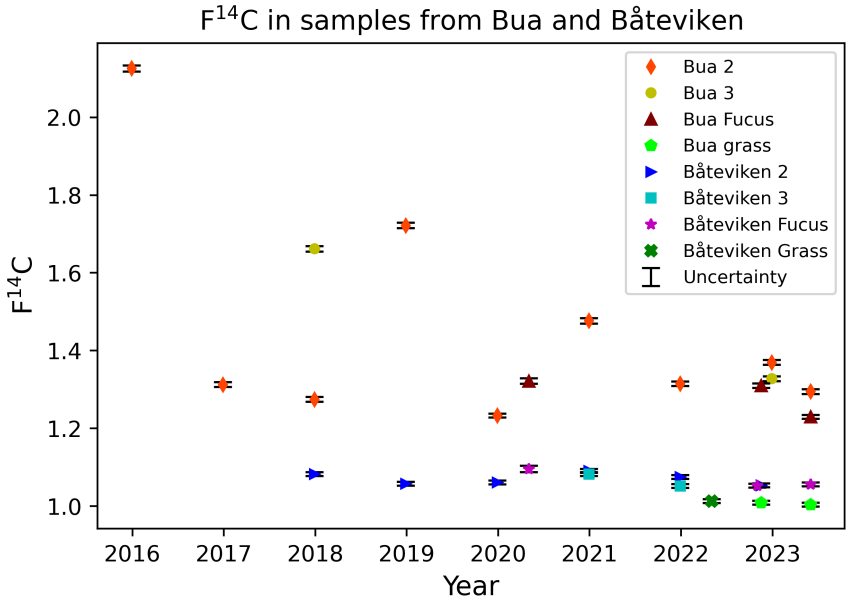

Figure 5.2: $F^{14}C$ in shells of mussels from Båteviken and Bua (by NPP), samples were taken from two shells at each site. $F^{14}C$ in seaweed "(*Fucus*)" (Stenström and Mattsson, 2022) and grass from the same locations is also included. The uncertainty marks the statistical error of the SSAMS measurements.

5.3 Blue mussels from Särdal

In Figure 5.3 and 5.4 $F^{14}C$ in the atmosphere, a modelled surface average of the ocean (down to 75 m), in seaweed, and in blue mussels shells are shown. It should be mentioned that the habitat of blue mussels is shallow waters, down to about 20 m below the surface, with the majority of them living in the intertidal zone (Havforskningsinstituttet, 2021). Both seaweed and mussel samples from this study have been picked in shallow water. Most of the seaweed data is unpublished, except the seaweed samples taken in 1967, which is from Stenström and Mattsson (2022).

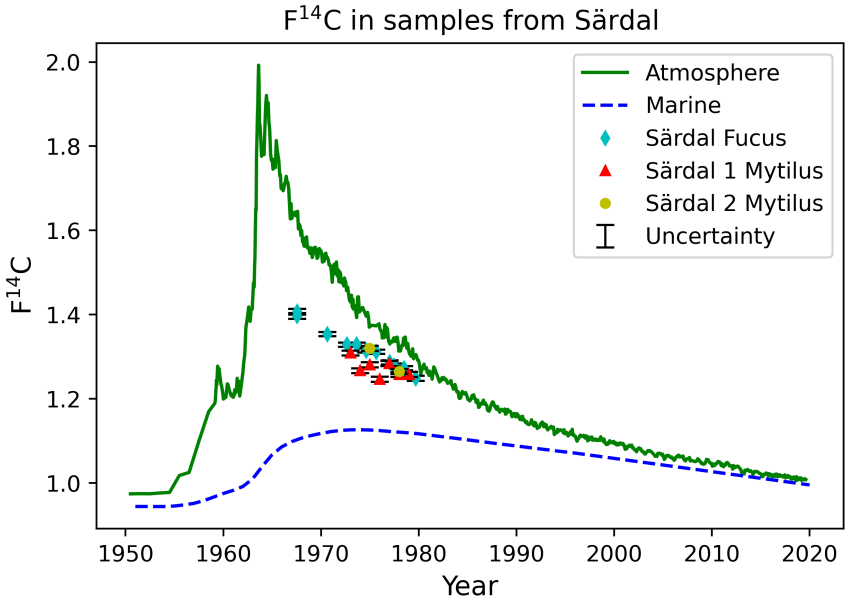

Figure 5.3: $F^{14}C$ in samples from the fibrous layer of *Mytilus edulis* and in *Fucus spp.* (Stenström and Mattsson, 2022) from Särdal. Atmospheric $F^{14}C$ based on data from (Emmenegger et al., 2020; Hammer and Levin, 2017; Levin and Kromer, 2004; Levin et al., 2013), and modelled marine $F^{14}C$ from (Reimer et al., 2009). The modelled marine $F^{14}C$ considers a global average of surface waters down to 75 m below the surface. The uncertainty marks the statistical error of the SSAMS measurements.

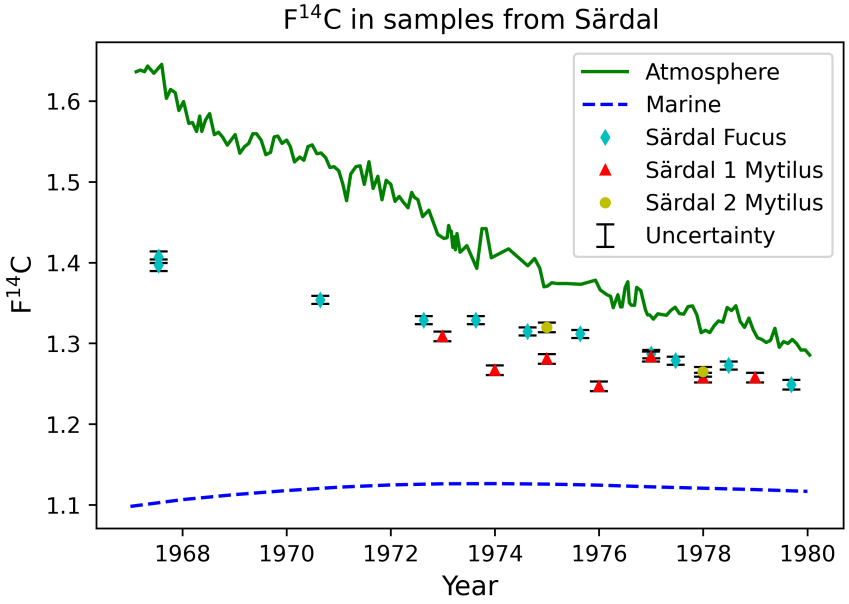

Figure 5.4: $F^{14}C$ in samples from the fibrous layer of *Mytilus edulis* and in *Fucus spp.* (Stenström and Mattsson, 2022) from Särdal. Atmospheric $F^{14}C$ based on data from (Emmenegger et al., 2020; Hammer and Levin, 2017; Levin and Kromer, 2004; Levin et al., 2013), and modelled marine $F^{14}C$ from (Reimer et al., 2009). The uncertainty marks the statistical error of the SSAMS measurements. Only the years from which there is mussel and seaweed data from Särdal is shown.

Chapter 6

Discussion

The largest contributing source of uncertainty regarding the results of this project is related to locating each annual band in the blue mussel shells. The SSAMS measurements have small uncertainties, especially for samples which are not particularly old, such as the samples in this study.

6.1 Age determination of blue mussel shells

As mentioned, the most prominent uncertainty in this study is by far the age determination of the blue mussels shells. The methods for identifying the annual shell structures are widely used, however the uncertainties of said methods are rather ambiguous. Furthermore, several of the scientific papers that were researched during this Bachelor's project do not clearly state their own methods. Instead they refer back to older articles and books, with a majority being based on Kennish et al. (1980); Clark (1980); and Lutz (1976). There is a study by Neves and Moyer (1988), which compares different methods for determining mussel age. For this study a different mussel species than *Mytilus edulis* was used and their results might not be directly applicable to blue mussel shells. It is still worth to mention that they did find a general trend towards assuming a younger age, when examining the external structure of shells.

Something that became apparent during the method development was that to recognise annual patterns in the shells one needs extensive training. In the acetate peels it was difficult to distinguish between annual growth marks and discoloration of the shell. This was evident even though the acetate peels made were of high quality capturing clear details. When regarding the external annual structures of the blue mussels, it was noted that older thicker shells were harder to determine the age of. The two main reasons for wrong estimates using this method (assuming one has the appropriate training to be successful) is fake annual structures and eroding of the fibrous layer (Neves and Moyer, 1988). If sand or other small particles get trapped within the periostracum during shell formation it might look like an annual ring, this will be more likely to have happened close to the posterior edge of old shells. As the shells grind against its surroundings the fibrous layer will get eroded, making it impossible to see the annual rings in the umbo region(Neves and Moyer, 1988).

There is a certain overlap between where one annual ring ends and the next one begins. To avoid having this interfere with the final results one could try to cut off the overlapping parts from each sample. In this project it was chosen not to do so as cutting the shells was challenging, especially when trying to cut off a narrow section perpendicular to the axis of maximal growth. Doing this with success would also require a great certainty of the location of each band. Cutting this off could also lead to data from a specific season of the year, the time when the growth rings form, never being analysed.

Next it was noted, when comparing the acetate peels to the markings of external structures, that the youngest annual growth band, located closest to the posterior edge of the shell, was

often missed when examining the external growth marks.

This agrees with the findings of Neves and Moyer (1988). However, this last annual ring was often located only millimetres from the posterior edge of the shells meaning that it would be hard to cut off without breaking this ring into pieces. Even if that could be done successfully it might not be a big enough piece of shell to provide a sample for AMS analysis.

The annual structures in the nacre, which is more easily identifiable within the acetate peels compared to those in the fibrous layer, agreed well with external age estimates for all samples. It can therefore be assumed that whether or not we found the exact location of each individual band is the major source of uncertainty not the total estimated age. If each band is slightly misplaced this will add

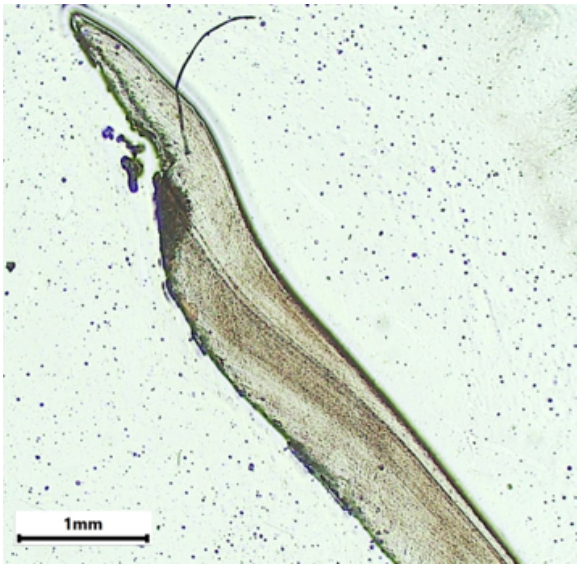

Figure 6.1: The youngest annual ring, which was not identified externally, from the Bua 2 sample. Picture by Anders Lindskog.

up, and in the worst case lead to an annual band being missed entirely. Together with the fact that the youngest growth band might have been entirely missed when dividing the shells. It can therefore be suspected that each of the samples, especially those towards by the umbo region, can be about one to two years older than what have been assumed.

If some of the nacre was not separated from the fibrous layer, as we suspected, this could also have interfered with the results. However, it is unlikly to have a big effect on the results due to how thin possible nacre was. Most likely it was corroded by the acid, and if some nacre was left on each shell piece the uncertainty due to this is negligible compared to the uncertainties related to the location of each annual ring. Though it should be mentioned that for one of the samples, specifically the year 2018 (ring 4) from Bua 2, it was somewhat harder to separate the nacre and the fibrous layer, which might have led to the nacre affecting this specific sample.

A measure which should be taken in the future is to measure the length of each shell segment during the pre-treatment. Furthermore several growth curves for similar conditions as there is at our sample sites should be found and used for size and age comparisons. Ideally we should make our own growth curves based on several individuals with known ages from each of the sample sites, e.g. by planting mussel larvae and collecting mussels from these during the following years. It should however be noted that when comparing our annual mussel growth to the annual growth within the mussels from Kullen (Dunca and Boalt, 2011) the slopes of the plots matches quite well, further supporting our age estimates.

It would also be interesting to do more testing in regards to heating shells at temperatures of 600 °C and higher to try and get the shells to properly separate along annual rings. However, this cannot be done without being more certain on exactly where the annual rings are located, otherwise there is no way of saying whether the shell separated along an annual rings, or some other irregularity in the shell.

6.2 $F^{14}C$ in Särdal

As showed in Figure 5.3 and 5.4 both shell and seaweed samples are influence by the bomb pulse. The $F^{14}C$ in the samples from Särdal decreases for the newer samples, following the bomb pulse value in the atmosphere. This is especially evident in the seaweed samples.

Blue mussels and seaweed live close to the ocean surface, which can explain the difference

between the amount of ^{14}C in the samples and the modelled marine value, which is based on an average for the upper 75 m of the ocean surface. If the seaweed was exposed to more air than the blue mussels, which is not unthinkable, this can also explain why the seaweed has a slightly higher level of ^{14}C. Additionally since the blue mussels feed on marine organisms this adds another carbon influence that the seaweed do not experience. Both the mussel shells and seaweed were picked by hand, from shallow waters (Stenström K. E., personal communication December 12th, 2023). This means that their habitat likely had a higher $F^{14}C$ value than what the modeled marine $F^{14}C$ from Reimer et al. (2009) shows. There is also a possibility that the samples were directly exposed to the atmosphere during low tide.

6.3 $F^{14}C$ in Bua

An interesting thing to note in Figure 5.2, is that the $F^{14}C$ levels for Bua jumps up and down a lot in-between years, while the $F^{14}C$ values in Båteviken are held quite stable. In addition relatively high amounts of ^{14}C detected in Bua (comparable to the maximum of the atmospheric bomb pulse in 1963). This agrees with Stenström and Mattsson (2022), which saw a peak in marine ^{14}C in the coastal region by Ringhals NPP (maximum $F^{14}C$ in seaweed of 1.322(7) in 2020), compared to other sites collected along the Swedish coast. Their findings prove that this NPP has a certain marine discharge of ^{14}C, something that is further supported by the findings of this project. Another interesting discovery is that the atmospheric values of ^{14}C by Ringhals NPP, as evaluated by the grass samples, are similar to those in Båteviken, far from any nuclear power plants.

Furthermore, if the assumed age for some of the annual rings is too low, one could e.g. compare the 2018 sample for Bua 3 to the 2019 sample for Bua 2, which have similar results for $F^{14}C$. Both 2023 mussel shell samples from Bua showed similar values of $F^{14}C$. Since this is the year when the shells were picked the uncertainty in age of these two samples are the lowest, supporting the validity of the method we have developed.

6.4 $F^{14}C$ in Båteviken

$F^{14}C$ in the seaweed and mussel shells from Båteviken are in agreement with each other. These samples show a higher specific activity than the grass, something that is due to marine discharge from two reprocessing plants for spent nuclear fuel, Sellafield in England and La Hague in France. Stenström and Mattsson (2022) found that out of these two, La Hague contributed the most to the ^{14}C excess measured in Båteviken. In general the further north along the Swedish west coast ^{14}C is measured, the more discharge from La Hague will affect the $F^{14}C$ value in the marine environment.

Chapter 7

Conclusion and outlook

7.1 Conclusion

First and foremost, everything points towards it being possible to use the annual structures of shells from blue mussels to get proxydata for marine discharges of ^{14}C from NPPs. While the method did work, it will need some further development, especially in regards to locating each annual band. To successfully do this we would need more practice locating annual structures in the shells, ideally we would want to consult an expert on blue mussel shells. However, the results obtained were corresponded to findings made by Stenström and Mattsson (2022), from seaweed along the Swedish west coast.

7.2 Outlook

Apart from finding and consulting an expert on *Mytilus edulis* shell structure, it would be interesting to consider other possible methods for identifying the annual shell structure. A possibility is, as mentioned in the discussion, to grow mussels in a controlled location at the sample sites, since the ages of these mussels would be known. Furthermore locating the annual bands using dendrochronology software could be tested. The main challenge with this approach would be to get enough data on what the annual structure looks like to be able to properly train the algorithm. Another approach to be considered is laser ablation analysis, a form of mass spectrometry, though this might have issues identifying different ions from a specific element, trials on using this to identify annual bands of blue mussels have been done. Lastly it would be interesting to study more samples from other sample sites.

Bibliography

(1974). Reaktorkemi. Studsviks kompendier: 9, published by AB Atomenergi Studsvik 1974.

Checa, A. and Salas, C. (2017). Treatise Online no. 93: Part N, Revised, Volume 1, Chapter 3: Periostracum and shell formation in the Bivalvia. *Treatise Online*.

Checa, A. G. (2018). Physical and biological determinants of the fabrication of molluscan shell microstructures. *Frontiers in Marine Science*, 5.

Clark, G. R. (1980). Appendix 1.2 study of molluscan shell structure and growth lines using thin sections. In Rhoads, D. C. and Lutz, R. A., editors, *Skeletal growth of aquatic organisms : biological records of environmental change*, pages 603–606. Plenum press, New York.

Connan, O. and Tack, K. (2010). Metals in marine environment (mollusc Patella sp., fish Labrus bergylta, crustacean Cancer pagurus, beach sand) in a nuclear area, the North Cotentin (France). *Environmental Monitoring and Assessment: An International Journal Devoted to Progress in the Use of Monitoring Data in Assessing Environmental Risks to Man and the Environment*, 165(1-4):67 – 86.

Dalbeck, P. C. (2007). *Crystallography, stable isotope and trace element analysis of Mytilus edulis shells in the context of ontogeny.* PhD thesis, University of Glasgow.

Druffel, E. M. and Suess, H. E. (1983). On the radiocarbon record in banded corals: Exchange parameters and net transport of 14co2 between atmosphere and surface ocean. *Journal of Geophysical Research: Oceans*, 88(C2):1271–1280.

Dunca, E. and Boalt, E. (2011). Samband mellan skaltillväxt och ålder hos blåmusslan (mytilus edulis) i Östersjön. *Rapport*.

Dunca, E., Mutvei, H., Göransson, P., Mörth, C.-M., Schöne, B. R., Whitehouse, M. J., Elfman, M., and Baden, S. P. (2009). Using ocean quahog (Arctica islandica) shells to reconstruct palaeoenvironment in Öresund, Kattegat and Skagerrak, Sweden. *International Journal of Earth Sciences: GR Geologische Rundschau*, 98(1):3 – 17.

Emmenegger, L., Leuenberger, M., and Steinbacher, M. (2020). Icos atc/cal 14c release, jungfraujoch (10.0 m), 2016-01-04–2019-08-11.

Fifield, L. K. (2005). *Electrostatic accelerators*, chapter 23 Accelerator Mass Spectroscopy, pages 461–485. Particle acceleration and detection. Springer, Berlin.

Forsgren, N. (2012). *Från ingenting alls till Ringhals : om tillkomsten av Sveriges största kraftverk.* Vattenfall Ringhals.

Georgiadou, E. A. (2014). *Exploring the possibilities of ^{1}C bomb-pulse dating of human tissue samples.* Division of Nuclear Physics, Department of Physics, Lund University.

Haag, W. R. and Commens-Carson, A. M. (2008). Testing the assumption of annual shell ring deposition in freshwater mussels. *Canadian Journal of Fisheries Aquatic Sciences*, 65(3):493 – 508.

Hammer, S. and Levin, I. (2017). Monthly mean atmospheric D14CO2 at Jungfraujoch and Schauinsland from 1986 to 2016.

Havforskningsinstituttet (2021). *Tema: Blåskjell*. hi.no. https://www.hi.no/hi/temasider/arter/blaskjell Updated: 29th of June 2021. Accessed: 15th of November 2023.

Henley, W. F. and Jones, J. W. (2020). Freshwater Mussel Shell Thin-Section Analyses for the Hudson River NRDA. Technical report, Hudson River Natural Resource Trustees, State of New York.

IAEA (2014). *Reference sheet for quality control materials*. Vienna International Centre, P.O. Box 100, 1400 Vienna, Austria.

Ji, K. (2022). *Hot Banana*. what-if.xkcd.com https://what-if.xkcd.com/158/ Accessed: 11th of November 2023.

Kautsky, N. (1982). Growth and size structure in a baltic mytilus edulis population. *Marine Biology*, 68(2):117–133.

Kennish, M. J., Rhoads, D. C., and Lutz, R. A. (1980). Appendix 1.1 preparation of acetate peels and fractured sections for observation of growth patterns within bivalve shell. In Rhoads, D. C. and Lutz, R. A., editors, *Skeletal growth of aquatic organisms : biological records of environmental change*, pages 597–601. Plenum press, New York.

Klody, G., Schroeder, J., Norton, G., Loger, R., Kitchen, R., and Sundquist, M. (2005). New results for single stage low energy carbon ams. *Nuclear Instruments and Methods in Physics Research Section B: Beam Interactions with Materials and Atoms*, 240(1):463–467. Accelerators in Applied Research and Technology.

Källberg, E. (2023). Näringsämnen och metaller i sediment och blåmusslor från Hanöbukten - En analys av marin miljöpåverkan från massabruk. Student Paper.

Levin, I. and Kromer, B. (2004). The tropospheric 14co2 level in mid-latitudes of the northern hemisphere (1959-2003). *Radiocarbon*, 46(3):1261 – 1272. Cited by: 442; All Open Access, Bronze Open Access, Green Open Access.

Levin, I., Kromer, B., and Hammer, S. (2013). Atmospheric 14co2 trend in western european background air from 2000 to 2012. *Tellus B: Chemical and Physical Meteorology*.

Lougheed, B. C., Filipsson, H. L., and Snowball, I. (2013). Large spatial variations in coastal ^{14}C reservoir age - a case study from the Baltic Sea. *Climate of the Past*, 9(3):1015–1028.

Lutz, R. A. (1976). Annual growth patterns in the inner shell layer of Mytilus edulis L. *Journal of the Marine Biological Association of the United Kingdom*, 56(3):723–731.

Magnusson, Å. (2007). *^{14}C Produced by Nuclear Power Reactors - Generation and Characterization of Gaseous, Liquid and Solid Waste*. PhD thesis, Lund University.

McGrorty, S. and Goss-Custard, J. D. (1993). Population dynamics of the mussel mytilus edulis along environmental gradients: Spatial variations in density-dependent mortalities. *Journal of Animal Ecology*, 62(3):415–427.

Meli, M. A., Desideri, D., Roselli, C., and Feduzi, L. (2008). Natural radioactivity in the mussel Mytilus galloprovincialis derived from the central Adriatic Sea (Italy). *Journal of Toxicology and Environmental Health - Part A: Current Issues*, 71(18):1270–1278 – 1278.

Mæhlum, L. (2023). *karbonpumpe*. Store Norske Leksikion. https://snl.no/karbonpumpe Accessed: 5th of December 2023.

National Academy of Science (1980). *The International Mussel Watch: Report of a Workshop*. 2101 Constitution Avenue, N.W. Washington, o.c. 20418.

Neves, R. and Moyer, S. (1988). Evaluation of techniques for age-determination of fresh-water mussels (unionidae). *American Malacological Bulletin*, 6(2):179 – 188.

Reimer, P., Baillie, M., Bard, E., Bayliss, A., Beck, J., Blackwell, P., Ramsey, C. B., Buck, C., Burr, G., Edwards, R., Friedrich, M., Grootes, P., Guilderson, T., Hajdas, I., Heaton, T., Hogg, A., Hughen, K., Kaiser, K., Kromer, B., McCormac, F., Manning, S., Reimer, R., Richards, D., Southon, J., Talamo, S., Turney, C., van der Plicht, J., and Weyhenmeyer, C. (2009). Intcal09 and marine09 radiocarbon age calibration curves, 0-50,000 years cal bp. *Radiocarbon*, 51(4):1111 – 1150. Cited by: 4095; All Open Access, Bronze Open Access, Green Open Access.

Rypel, A. L., Haag, W. R., and Findlay, R. H. (2008). Validation of annual growth rings in freshwater mussel shells using cross dating. *Canadian Journal of Fisheries Aquatic Sciences*, 65(10):2224 – 2232.

Schöne, B. R., Fiebig, J., Pfeiffer, M., Gle, R., Hickson, J., Johnson, A. L., Dreyer, W., and Oschmann, W. (2005). Climate records from a bivalved Methuselah (Arctica islandica, Mollusca; Iceland). *Palaeogeography, Palaeoclimatology, Palaeoecology*, 228(1):130 – 148.

Scourse, J., Butler, P., Richardson, C., Wanamaker, A., Weidman, C., Heinemeier, J., Reimer, P., and Witbaard, R. (2012). The marine radiocarbon bomb pulse across the temperate North Atlantic: A compilation of Δ14C time histories from Arctica islandica growth increments. *Radiocarbon*, 54(2):165–186 – 186.

Seed, R. (1980). Chapter 1: Shell growth and form in the bivalvia. In Rhoads, D. C. and Lutz, R. A., editors, *Skeletal growth of aquatic organisms : biological records of environmental change*, pages 23–67. Plenum press, New York.

Skog, G. (2007). The single stage ams machine at lund university: Status report. *Nuclear Instruments and Methods in Physics Research Section B: Beam Interactions with Materials and Atoms*, 259(1):1–6. Accelerator Mass Spectrometry.

SSM (2021a). *Så fungerar ett kärnkraftverk*. Stralsakerhetsmyndigheten.se. https://www.stralsakerhetsmyndigheten.se/omraden/karnkraft/sa-fungerar-ett-karnkraftverk/ Accessed: 4th of December 2023.

SSM (2021b). *Ringhals kärnkraftverk*. Stralsakerhetsmyndigheten.se. https://www.stralsakerhetsmyndigheten.se/omraden/karnkraft/karntekniska-anlaggningar-i-drift-i-sverige/ringhals/ Accessed: 5th of December 2023.

SSM (2023). *Regler*. Stralsakerhetsmyndigheten.se. https://www.stralsakerhetsmyndigheten.se/regler/ Accessed: 11th of November 2023.

SSMFS (2008:23). *Strålsäkerhetsmyndighetens föreskrifter om skydd av människors hälsa och miljön vid utsläpp av radioaktiva ämnen från vissa kärntekniska anläggningar*. https://www.stralsakerhetsmyndigheten.se/contentassets/54597d9d80e0480f8ea

97221fc78c0dd/ssmfs-200823-stralsakerhetsmyndighetens-foreskrifter-om-skydd-av-manniskors-halsa-och-miljon-vid-utslapp-av-radioaktiva-amnen-fran-vissa-karntekniska-anlaggningar-konsoliderad-version.pdf.

SSMFS (2021:6). *Strålsäkerhetsmyndighetens föreskrifter och allmänna råd om drift av kärnkraftsreaktorer*. https://www.stralsakerhetsmyndigheten.se/contentassets/80946ac596624f45a977e0dc0efbb9be/ssmfs-20216-stralsakerhetsmyndighetens-foreskrifter-och-allmanna-rad-om-drift-av-karnkraftsreaktorer.pdf.

Stenström, K., Skog, G., Georgiadou, E., Genberg, J., and Mellström, A. (2011). *A guide to radiocarbon units and calculations*. LUNFD6(NFFR-3111)/1-17/(2011). Lund University, Nuclear Physics.

Stenström, K. E. (2015). Beam transport. Course material for *Experimental tools - FYSN15* at Lund University.

Stenström, K. E. and Mattsson, S. (2022). Spatial and temporal variations of 14c in fucus spp. in swedish coastal waters. *Journal of Environmental Radioactivity*, 242:106794.

Sterrett, S. S. and Saville, L. D. (1974). A technique to separate the annual layers of a naias shell (Mollusca, Bivalvia, Unionacea) for analysis by neutron activation. *Bulletin of the Amarican Malacological Union*, pages 55–57.

Tevesz, M. J. S. and Carter, J. G. (1980). Appendix 1.4 study of annual growth bands in unionacean bivalves. In Rhoads, D. C. and Lutz, R. A., editors, *Skeletal growth of aquatic organisms : biological records of environmental change*, pages 613–614. Plenum press, New York.

Tierney, K. M. (2017). Marine ecosystem uptake of nuclear reprocessing derived radiocarbon (^{14}C).

Wacker, L., Němec, M., and Bourquin, J. (2010). A revolutionary graphitisation system: Fully automated, compact and simple. *Nuclear Instruments and Methods in Physics Research Section B: Beam Interactions with Materials and Atoms*, 268(7):931–934. Proceedings of the Eleventh International Conference on Accelerator Mass Spectrometry.

Weidman, C. R. and Jones, G. A. (1993). A shell-derived time history of bomb ^{14}C on Georges Bank and its Labrador Sea implications. *Journal of Geophysical Research: Oceans*, 98(C8):14577–14588.

Weisser, D. C. (2013). *Encyclopedia of nuclear physics and its applications*, chapter 3 Electrostatic accelerators, pages 106–109. Wiley-VCH, Weinheim, Bergstr.

Appendix A

Step-by-step method for sample preparation

1. Remove the periostracum.
    - Filing of the periostracum can be done e.g. with a Dremel with a diamond-tipped engraving bit (available at the Department of Geology, Lund University).
2. Mark the annual rings.
    - The rings are easier to see if the shell is illuminated, preferable having the light source on the inside of each shell valve. In this case a strong head lamp lying face up on a table was used.
    - Do this before heating the shell, since the light might not shine through the shell as well after the shell is heated. Make sure that the marker does not contain carbon.
3. Cut the shell for heating and making of acetate peels.
    - A lapidary saw with a Diamond Cut Off Wheel, the B4D20 blade from Struers ApS, can be used for the cutting (available at the Department of Geology, Lund University).
    - To better be able to separate the nacre and the fibrous layer the posterior and anterior margin of the shell should be cut off, see figure A.1.
    - Use one of the cut edge pieces when making acetate peels.

Figure A.1: Example of how the shells were cut.

4. Make acetate peels.
    - Firstly identify which edge on the middle piece of the cut shell is closest to the line of maximal growth.
    - Polish the cut edge of the shell. in this case using a polishing machine with a 1200 grit disc, the model of the machine being RotoPol-25 by Struers ApS.
    - Wash the shell with distilled water and let it dry.
    - Put the cut edge in 2% HCl for 40 seconds.
    - Wash the shell with distilled water and let it dry.
    - Cut out a piece from a cellulose-film big enough to fit the shell, and pin it down flat on a table. (The cellulose film used was found without its packaging in a cabinet and therefore the exact brand is not known.)
    - Pour acetone on the cut edge of the shell and press the shell onto the film. Leave it until the acetone has vaporised.
    - Put the acetate peels between two microscope glass slides, to better be able to view them in the microscope.
5. Identify the annual rings in the acetate peel and compare them to what was found when illuminating the shell in step 2.
    - Additionally comparing the number of annual growth layers seen in the nacre to the amount of rings marked on the outside of the shell is advised, as the growth layers are usually more apparent in the nacre.
6. Divide the middle shell section according to the annual rings.
    - If needed re-draw the markings on the shell before cutting.
    - A Dremel with a diamond cutting blade rotating on slow speed, can be used for the cutting (available at the Department of Geology, Lund University).
7. Heat the shell for 10 minutes at 500 °C in air in an oven.
    - This should make the nacre and the fibrous layer of the shell split apart.
    - Let the shells cool.
8. Put the fibrous layer in acid to remove as much as possible of what is left of the nacre.
    - Included in the normal pre-treatment method of shells at the Lund Radiocabon Dating Laboratory, and was therefore done by personnel there. See Appendix B.

Appendix B

Sample pre-treatment for shells and other carbonates

Note that this method was not developed by me, and all steps explained here were performed by personnel at the Lund Radiocabon Dating Laboratory. It is included for transparicy, with permission from personnel at the Lund Radiocabon Dating Laboratory. Translated into English by me.

Treatment should be done right before graphitisation; if needed the samples can be kept in argon gas for a few days.
"Special mixture of HCl for shells" = 10 ml 37% HCl diluted with deionised water to 1000ml mixture.

1. Brush the shells clean.
2. Weight out a suitable amount. There is no need to treat more than 300 mg of the shell.
3. Put the shells in an ultrasonic cleaner with boiled deionised water for ca 5 min. *Important to boil the water to get rid of free* CO_2.
4. Dry the shells in a heating cabinet and weigh them again. If the shell weighs less than 10 mg you should not preform the following steps of the pre-treatment.
5. The "special mixture" is added in proportion to the weight of the shells.
   - Weight 150-300 mg. [(weight of the shell)/20] ml "special mixture" HCl is added.
   - Weight 80-150 mg. [(weight of the shell)/40] ml "special mixture" HCl is added*.
   - Weight 10-80 mg. [(weight of the shell)/60] ml "special mixture" HCl is added*.

   After ca 3 h in 80 ° the HCl should (mostly) have been consumed and 30%, 20%, or 10% respectively of the outer parts of the shell should be corroded by the solution.
6. Put the shells in an ultrasonic cleaner with boiled deionised water for ca 5 min.
7. Dry the shells in a heating cabinet at 110 °C.
8. If the shell weighs more than 20 mg mortar it.

* if needed add deionised water to get an appropite amount of liquid.

Appendix C

Sample data

Data regarding the samples sent in for SSAMs analysis at the Lund Radiocabon Dating Laboratory. The difference in assumed year for the annual bands in samples from the same year and location is due to difference in shell sizes. For example if two shells picked at the same time and place have four and six annual bands then band number two, counted from the umbo towards the posterior edge, will be two and four years old respectively.

Table C.1: Data regarding the samples sent in for analysis. When numbering the annual bands they were counted from the umbo towards the posterier edge, meaning that bands with a lower number are older.

Location	**Date picked**	**Latitude**	**Longitude**	**Annual ring (assumed year)**	**Weight before acid treatment [mg]**	**Weight after acid treatment [mg]**	**Segment length [mm ±1]**	**$F^{14}C$**
Båteviken	2022 Oct. 12	58.95 N	11.13 E	1 (2017)	29.0	24.7	15	1.083(5)
				2 (2018)	51.9	48.0	12	1.058(5)
				3 (2019)	73.8	68.1	11	1.061(5)
				4 (2020)	184.4	128.5	12	1.091(5)
				5 (2021)	216.5	149.1	7	1.075(5)
				6 (2022)	46.3	41.3	4	1.054(5)
Båteviken	2022 Oct. 12	58.95 N	11.13 E	2 (2020)	24.8	21.8	10	1.083(5)
				3 (2021)	83.3	71.1	12	1.052(5)
Särdal	1978 Dec. 24	56.76 N	12.63 E	1 (1972)	58.3	52.4	10	1.309(6)
				2 (1973)	101.6	87.8	12	1.267(6)
				3 (1974)	189.1	133.9	15	1.281(6)
				4 (1975)	128.9	110.1	8	1.247(6)
				5 (1976)	287.7	205.5	12	1.284(6)
				6 (1977)	289.5	217.9	8	1.258(6)
				7 (1978)	132.5	114.0	5	1.258(6)
Särdal	1978 Dec. 12	56.76 N	12.63 E	2 (1974)	69.0	62.88	13	1.320(6)
				5 (1977)	155.9	112.3	7	1.265(6)
Bua (by NPP)	2023 May 12	57.24 N	12.10 E	1 (2015)	29.7	27.5	10	2.126(8)
				2 (2016)	37.9	34.8	7	1.313(6)
				3 (2017)	94.1	81.7	11	1.275(6)
				4 (2018)	151.6	107.3	11	1.722(7)
				5 (2019)	223.7	162.5	12	1.233(5)
				6 (2020)	343.8	256.6	14	1.477(7)
				7 (2021)	198.4	142.4	7	1.315(6)
				8 (2022)	182.4	131.1	5	1.370(6)
				9 (2023)	182.4	130.7	6	1.295(6)
Bua (by NPP)	2023 May 12	57.24 N	12.10 E	2 (2017)	65.3	60.2	13	1.662(7)
				7 (2022)	266.2	190.7	7	1.328(6)